Analysis of LIF and Mie signals from single micrometric droplets for instantaneous droplet sizing in sprays

Koegl, Matthias; Hofbeck, Bernhard; Baderschneider, Kevin; Mishra, Yogeshwar Nath; Huber, Franz J.T.; Berrocal, Edouard; Will, Stefan; Zigan, Lars

Published in:
Optics Express

DOI:
10.1364/OE.26.031750

2018

Document Version:
Publisher's PDF, also known as Version of record

Research Article | Vol. 26, No. 24 | 26 Nov 2018 | OPTICS EXPRESS 31750
Optics EXPRESS

Analysis of LIF and Mie signals from single micrometric droplets for instantaneous droplet sizing in sprays

MATTHIAS KOEGL,[1,2,*] BERNHARD HOFBECK,[1] KEVIN BADERSCHNEIDER,[1] YOGESHWAR NATH MISHRA,[1] FRANZ J. T. HUBER,[1,2] EDOUARD BERROCAL,[2,3] STEFAN WILL,[1,2] AND LARS ZIGAN[1,2]

[1]*Lehrstuhl für Technische Thermodynamik (LTT), Friedrich-Alexander-Universität Erlangen-Nürnberg (FAU), 91058 Erlangen, Germany*
[2]*Erlangen Graduate School in Advanced Optical Technologies, FAU, 91052 Erlangen, Germany*
[3]*Division of Combustion Physics, Lund University, Box 118, Lund 22100, Sweden*
**matthias.koegl@fau.de*

Abstract: Planar droplet sizing (PDS) is a technique relying on the assumption that laser-induced fluorescence (LIF) and Mie scattering optical signals from spherical droplets depend on their volume and surface area, respectively. In this article, we verify the validity of this assumption by experimentally analyzing the light intensity of the LIF and Mie optical signals from micrometric droplets as a function of their diameter. The size of the droplets is controlled using a new flow-focusing monodisperse droplet generator capable of producing droplets of the desired size in the range of 21 µm to 60 µm. Ethanol droplets doped with eosin dye and excited at 532 nm are considered in this study, and the individual droplets were imaged simultaneously at microscopic and macroscopic scale. The effects of laser power, dye concentration, and temperature variation are systematically studied as a function of LIF/Mie ratio in the whole range of droplet sizes. Finally, a calibration curve at tracer concentration of 0.5 vol% is deduced and used to extract the droplet Sauter mean diameter (SMD) from instantaneous images of a transient ethanol spray. This droplet size mapping is done using structured laser illumination planar imaging (SLIPI), in order to suppress the artifacts induced by multiple light scattering.

1. Introduction

Laser sheet-based LIF /Mie ratio imaging is a technique created in 1993 for two-dimensional mapping of droplet size [1]. Since then the method has been applied for different types of sprays either named as Laser Sheet Dropsizing [2] or Planar Droplet Sizing (PDS). The approach is based on the intensity ratio of liquid LIF intensity to the Mie intensity from the probed spray region. Note that some other researchers have proposed the Raman/Mie ratio for droplet sizing [3] or the LIEF/Mie ratio (LIEF: Laser-Induced Exciplex Fluorescence) [4], and droplet lasing-based sizing [5]. In PDS it is assumed that LIF and Mie intensities from the droplets are proportional to d^3 and d^2, respectively [1,2], where d is the droplet diameter. These dependencies have been discussed by several researchers [6–13], yet these investigations have been computational in the majority and their experimental validations are usually for droplet diameters greater than 100 µm [6–12,14]. For example, Domann *et al.* investigated the parameters influencing the accuracy of the PDS approach with a combined theoretical and experimental study with the monodisperse water droplet sizes ranging from 170 to 270 µm [14]. It was found that Mie signal showed a good agreement with d^2, however, in LIF, the d^3 dependency was valid only for the lowest dye (Rhodamine 6G) concentration used and the d - exponent changed from 3 to 2 with an increase in dye concentration from 0.001 to 0.1 g/L.

#341899 https://doi.org/10.1364/OE.26.031750
Journal © 2018 Received 9 Aug 2018; revised 20 Oct 2018; accepted 20 Oct 2018; published 16 Nov 2018

Optics EXPRESS

Another numerical study by Frackowiak *et al*. [10] confirmed this behavior as for a low absorbing mixture the LIF-signal obeyed the d^3 law, while for highly absorbing mixtures a d^2 relation was more favorable. Charalampous *et al*. [12] numerically investigated the d^3 and d^2 dependencies as a function of collection angle, dye concentration, and real part of the refractive index. It was concluded that for LIF the d^3 dependency was adhered to for the lowest dye (Rhodamine 6G) concentration of 0.001g/L and real refractive index variation had a very little effect. For Mie-scattering, it was found that the d^2 function depends strongly on the real refractive index, scattering angle, and dye concentration. The relation was best respected for lowest dye concentration, and scattering detection at 60° collection angle, for all droplet refractive indices. Therefore, the selection of LIF tracer and its concentration are essential to the accuracy of the LIF/Mie ratio technique. In addition, the influence of temperature and laser fluence on tracer LIF spectrum must be also characterized [15]. The effect of laser fluence on the LIF/Mie ratio is must be known for considering laser fluctuations (both shot-to-shot and spatial variations). Furthermore, the temperature of the droplets is often not known exactly. It may change during evaporation (due to heating of the droplets in the hot gas or due to cooling induced by the evaporation enthalpy). Thus, also the dye concentration will change during droplet evaporation.

In the past, tracers such as TMPD [16], naphthalene [17], Rhodamine [18,19], fluorescein [20], 3-pentanone [21,22], and triethylamine [23] have been used both in liquid and in vapor phases. Recently, the eosin dye has been found as a suitable dye tracer for LIF imaging in ethanol sprays [24–26]. In this work, it was also used because of its high quantum yield of ~ 0.68 in ethanol at 500 nm excitation [27]. Moreover, the quantum efficiency of the modern sCMOS image sensor is usually the highest (~ 60%) within the LIF emission spectrum of the eosin in ethanol solution (maximum at 550 nm).

To calibrate the LIF/Mie ratio, Phase Doppler Anemometry (PDA) was largely used in the past [6,28–34]. However, PDA instruments measure temporally varying spray drop sizes at a single point, which is convenient for time-averaged measurements. Using a monodispersed droplet generator instead allows extracting the single-shot LIF/Mie ratio [35]. This second approach is more adequate for the calibration of instantaneous images. However, despite many reported investigations on LIF/Mie ratio calibration using monodisperse droplet generators, a thorough experimental study on d^3 dependence of LIF, and d^2 dependence of Mie is still missing for $d \leq 50$ µm (which is relevant for engine sprays) along with varying influencing parameters such as droplet diameter, dye concentration, laser power, and droplet temperature *etc*. For example, Park *et al*. performed microscopic calibration of LIF/Mie ratio with 20 images averaged for each droplet of fluorescing unleaded gasoline produced in 50-300 µm size range [36]. Le Gal *et al*. reported macroscopic calibration of LIF/Mie ratio from the individual droplets of self-fluorescent 'mineral spirit' produced in the sizes range of 50-180 µm [2]. These droplet size ranges are not satisfactory for most cases of atomizing sprays, especially those used in for combustion applications.

In this article, we report simultaneous microscopic and macroscopic LIF/Mie measurements from a novel flow-focusing monodisperse droplet generator, for accurate calibration of instantaneous droplet sizing measurement. The experimental investigation is performed as follows: (i) Using the microscopic/macroscopic setup, the LIF and Mie signals are recorded simultaneously from each individual droplet of dye-doped ethanol to respectively evaluate their d^3 and d^2 dependence for 21 µm $\leq d \leq$ 60 µm. (ii) The dependence of the LIF/Mie ratio on laser energy, dye concentration and the temperature is thoroughly investigated, in particular also to assess possible errors in the results due to variations or uncertainties in the process parameters. (iii) The derived calibration curve is used for sizing droplets in an ethanol DISI spray on a single-shot basis. This needs single droplet calibration data as PDA only provides averaged information in a limited SMD-range. To face measurement errors introduced by multiple light scattering while generating instantaneous spray images, the two-phase SLIPI (2p-SLIPI) approach [24,26] is employed here when

Optics EXPRESS

recording the LIF and Mie images. (iv) Finally, a discussion of uncertainties of the Mie-scattering data is provided.

2. Description of the experiment

2.1 Microscopic and macroscopic LIF/Mie optical setup

The optical arrangement of the microscopic and macroscopic LIF/Mie droplet sizing setup in combination with 2p-SLIPI setup is shown in Fig. 1. Three laser pulses of 532 nm wavelength from an Nd:YAG laser cluster (Thales, France) with top hat beam profiles are used. Two of the laser pulses are used for 2p-SLIPI optical setup in the spray chamber, as described in detail in [24]. The third laser pulse is used for simultaneous microscopic and macroscopic investigations applied for studying the droplet stream produced by the droplet generator. The LIF and Mie light intensity is recorded with two micro and macro objective systems, each of them equipped with two identical scientific CMOS cameras (LaVision GmbH, Germany). Each recorded image corresponds to 2560 x 2160 pixels. The microscopic objective system is equipped with a long range microscope (Infinity, model K2 DistaMax) with the region of interest equal to 0.71 mm x 0.60 mm and with a pixel resolution of 3.63 pixel/µm). The incoming signal is separated just behind the objective by a cube beam splitter (70% transmission for the LIF signal and 30% reflection for the Mie signal) into two signals. The adjustment possibilities of the systems simplify the alignment to obtain the same field-of-view on both cameras.

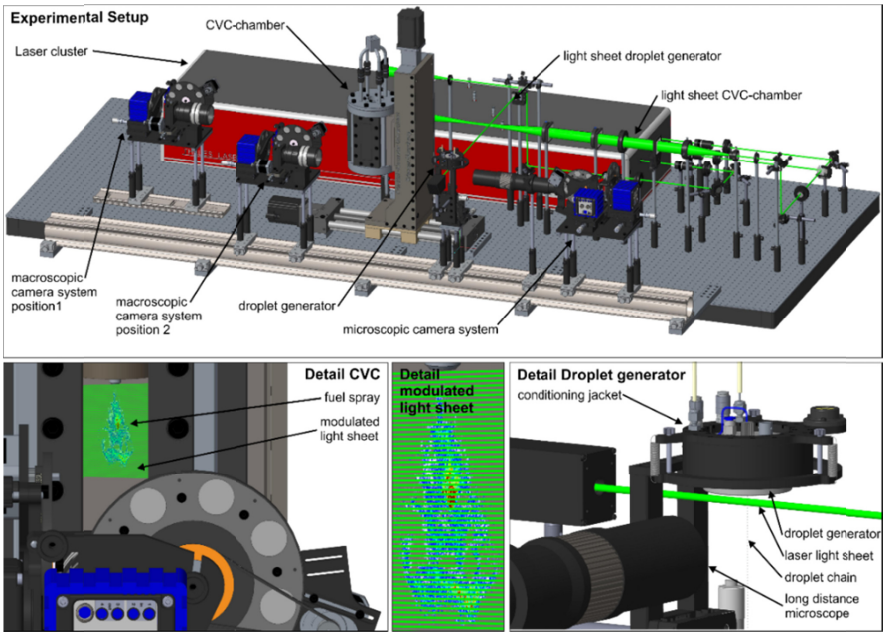

Fig. 1. Optical arrangement of the simultaneous microscopic and macroscopic LIF/Mie setup in combination with 2p-SLIPI (top). Detailed spray chamber with modulated light sheet and droplet generator view (bottom).

For the fluorescence, an organic luminescence dye, eosin (Sigma Aldrich) is added with 0.5 vol% to the liquid fuel, ethanol. The excited liquid solution using 532 nm, emits a broadband signal between 540 and 680 nm. The LIF emission is detected by using a 532 nm (17 nm FWHM) notch filter to exclude the excitation wavelength. The Mie scattering signal is detected by using a 532 nm (1 nm FWHM) laser line pass filter. To optimize the LIF and Mie intensity further on the camera systems, a motorized filter wheel is fixed in front of the camera chips. The wheel consists of neutral density (ND) filters of different optical densities

Optics EXPRESS

allowing for the best possible signal to noise ratios at constant laser power. All optical components such as optical filters, ND filters, and beam splitters are characterized by a spectrometer (Perkin Elmer, UV/VIS Spectrometer, type Lambda 40).

The macroscopic objective system is equipped with a 135 mm objective (Pentagon 2.8/135). The pixel resolution achieved in this case is 0.15 pixels/µm. This setup is fixed just opposite to the microscopic imaging system to perform simultaneous macroscopic evaluations synchronized with the microscopic detection. It is also equipped with the identical optical filters, beam splitter used in the microscopic objective system.

2.3 Monodisperse droplet generator

The monodisperse droplet generator is made by MSP Corp (Type 1530) and is reported to generate droplet of size ranging between 15 and 150 µm for methanol and water using the flow focusing concept [37]. This enables a rough adjustment of the average droplet size without any modification of the droplet generator. In this device, the droplet size is changed by fuel mass flow and piezo frequency in contrast to the orifice droplet generators. The flow focusing air and the fuel are kept at 298 K to enable constant conditions during the measurements at an ambient pressure of 0.1 MPa. The temperatures of the whole setup are monitored by integrated thermocouples (type K). The downstream distance between the droplet generator orifice and droplet measurement plane is between 3 and 7 mm depending on the droplet size.

2.4 CVC-chamber

The constant volume combustion (CVC) chamber is used to investigate DISI-sprays under engine-like conditions. It is operated with dry air at 0.2 MPa pressure and 298 K temperature, which represents a high load engine operating point. The ambient temperature in the CVC and the fuel temperature are set to 298K. The injector is heated by an integrated fluid-based heating circulator. The temperature of the nozzle tip is monitored with a highly sensitive micro sheathed thermocouple (0.25 mm diameter, type K). It is assumed that the fuel adopts the injector temperature due to the long residence time of the fuel in the injector (the injection duration is relatively short (1800 µs) for an injection repetition rate of 0.5 Hz. The chosen temperature range is also relevant for cold and warm start conditions of the engine sprays. The injection pressure is set to 16 MPa. A 5-hole DISI-injector (Bosch GmbH, Germany) is utilized, where one jet is centrally separated from others allowing unrestricted optical access. The physical parameters of the fuel ethanol are listed in Table 1. It should be noted that the dye concentration within the droplet could change due to evaporation. However, the studied conditions at moderate ambient temperatures lead to low evaporation rates. Thus, a strong variation of the dye concentration can be excluded. The temperature dependence of the LIF-signal is negligible at the investigated conditions. A detailed uncertainty analysis in the measurement due to changes in the dye concentration and temperature dependence of LIF can be found in [34]. For a wide temperature range, the LIF/Mie-ratio dependency will be addressed in the subsequent sections.

Table 1. Physical and chemical properties of ethanol [37–41]

Fuel	ethanol
H/C - ratio / O/C – ratio	3.0 / 0.5
Normal boiling point (K)	351.5
Density (g/cm^3) @ 298 K, 0.2 MPa	0.801
Surface tension @ 293 K (N/m)	0.0223
Heat of vaporization @ 293 K (kJ/kg)	929.6
Kin. viscosity @ 298 K, 0.2 MPa (m^2/s)	1.30 x 10^{-6}
Refractive index at 293 K (-)	1.36

Optics EXPRESS

3. Results from single droplet measurements

3.1 Image post-processing routine

In principle, the different diameters of droplets from the droplet generator are achieved by varying different parameters such as flow rate of the focusing air, the fuel mass flow and the frequency of the piezo crystal as mentioned in subsection 2.3. However, in practice, different droplet sizes are adjusted and measured by varying parameters in combination with the post-processing of the LIF images recorded from the microscopic LIF-setup. During the calibration, the droplet size is always controlled and re-adjusted for all fuel temperatures, laser fluences, dye concentrations etc.

Each individual droplet from the droplet generator is evaluated in terms of size, sphericity, location within the ROI (region of interest) and spacing between two droplets using the LIF image of the microscopic camera system. Only droplets which can be resolved within both microscope and macroscopic detection along with sphericity of 1 to 1.2 (major/minor axis ratio of the ellipse) are considered. The intensities of the LIF- and the Mie-signals for each individual droplet of different diameters are summed up. Each measurement is repeated five times with 2000 images covering droplet sizes of 25, 30, 37.5, 45, 52.5, 60 and 67.5 µm, respectively. A total of 33,510 individual droplets are considered for the evaluations at room temperature. For the evaluation of the intensities I of the LIF-and Mie-signals as a function of droplet diameter d, the two parameters are fitted according to the power-law function $I = a \cdot d^b$. As for different droplet sizes, a wide spread of intensities is expected from the power-law, the fit is performed by a weighted least square minimization, where the weighting factors are determined by the measurement noise of the signal σ_I. As the noise is distributed approximately log-normal, the minimization is performed in log-space. The weighting factors are then indirectly proportional to the noise level $1/\sigma_I^2$. By this routine, fitting errors caused by a greater weight of high intensities, corresponding to large droplets, are avoided.

3.2 Microscopic measurements

Figure 2 shows the bin-wise averaged LIF and Mie droplet signals from 25 µm to 60 µm ($d_{droplet}$ ± 0.25 µm). The droplet generator produces much larger fluctuations in droplet size but these were sorted out by the post-processing algorithm. The eosin concentration is set to 0.5 vol% of ethanol at constant laser power and fuel temperature of 293 K. Laser light enters the droplets from the left side shown in Fig. 2. The average droplet images are scaled up to ensure visibility. At certain droplet sizes, glare points become visible within the LIF images. There are also coinciding modes MDRs (Morphology- Dependent Resonances) evident in droplet LIF images [42,43]. The MDRs usually appear for small droplets when illuminated with high laser fluence. The Mie images consist exclusively of two glare points. Due to the extinction of light within the droplet, the intensity of the entrance glare point (reflection) is higher in comparison to the exiting glare point (refraction).

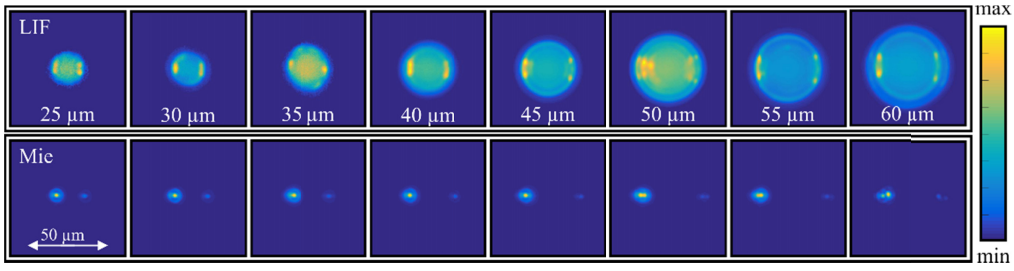

Fig. 2. Averaged LIF and Mie optical signals from micro-droplets in diameter ranging from 25 µm to 60 µm. The intensity of each image is normalized to their individual maximum value. Note that there are glare points and coinciding MDR modes on the LIF images, while only glare points visible on Mie images.

Optics EXPRESS

Figure 3 shows the fitting curves of the individual LIF and Mie signals and the LIF/Mie ratio deduced as a function of droplet diameter with their corresponding standard deviations.

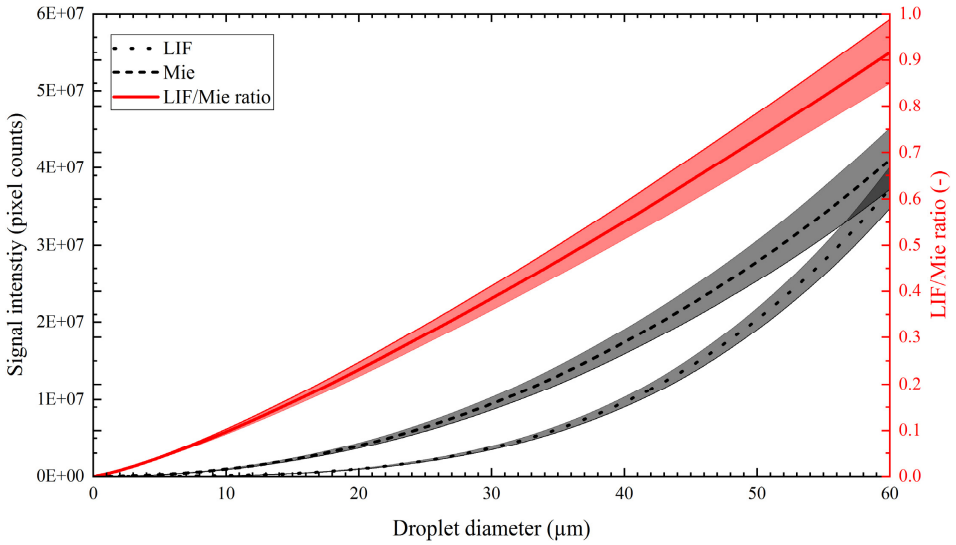

Fig. 3. The fitting curve of the experimental data plotted for LIF, Mie and LIF/Mie ratio as a function of droplet diameter for the reference conditions (1 MPa, 293 K, eosin concentration in ethanol: 0.5 vol %) with their corresponding standard deviations.

The LIF signal shows a volumetric trend and in our experiments, it is not very sensitive to the variation of the detection angle. The fitting curve roughly follows the d^3 dependence predicted by the literature [6–12,14]. It can be described by the following equation (power law) at standard conditions:

$$I_{LIF} = f(d_{droplet}) = 43.94 \cdot d_{droplet}^{3.33} \quad (1)$$

An exponent greater than three is mainly attributed to the glare points and MDRs emission in droplets. Le Gal *et al*. have reported MDRs as super-radiant effects in LIF/Mie ratio laser sheet drop sizing [2]. However, the effects of MDRs in macroscopic LIF/Mie ratio is found to have negligible influence on the droplet sizing because intensity peaks of the MDRs in both LIF and Mie signals should cancel out each other. The fitting curve of the Mie signal can be described with the following equation:

$$I_{Mie} = f(d_{droplet}) = 7062.5 \cdot d_{droplet}^{2.12} \quad (2)$$

The Mie-signal fitting curve shows a good agreement with the d^2 dependence according to the literature. Nevertheless, an exponent greater than two is also reported by Le Gal *et al*. [2] due to MDRs. The corresponding LIF/Mie ratio follows the function:

$$I_{\frac{LIF}{Mie}} = f(d_{droplet}) = 0.0054 \cdot d_{droplet}^{1.25} \quad (3)$$

The fitting curve in this study roughly exhibits the *d*-dependence according to the hypothesis of LIF/Mie droplet sizing approach [2,6]. In Table 2, the respective average pre-factors, exponents and standard deviations of the three fitting curves (LIF, Mie, LIF/Mie) are summarized for the reference conditions (293 K, 0.5 vol % eosin). Here, the uncertainty for the pre-factor *"A"* is given by the geometric standard deviation, i.e. the *1-σ* interval is from *[A*σ; A/σ]*. For the exponent *b,* the uncertainty is the arithmetic standard deviation, i.e. the *1-σ* interval is from *[b-σb; b + σb]*. The average values and standard deviation were calculated

Optics EXPRESS

from five individual calibration curves. The standard errors of the exponents show a lower variation for the LIF signal fit in comparison to the Mie signal fit. This behavior is caused by the detection angle dependence of the Mie signal in contrast to the LIF signal, which results in a wider signal distribution (see also discussion in section 6).

Table 2. Curve fitting parameters including average pre-factors and exponents as well as respective standard deviations for microscopic measurements of ethanol droplet (0.5 vol % eosin, 293 K).

signal fit	*Pre-factor A*	geom. std. deviation *a*	*Exponent b*	std. deviation *b*
LIF	43.939	1.0317	3.3346	0.0084
Mie	7062.5	1.0471	2.1166	0.0123
LIF/Mie ratio	0.0054	1.0371	1.2539	0.0096

In Fig. 4 the LIF/Mie ratio fitting curve is illustrated for the reference conditions with the corresponding experimental data. The uncertainty of the calibration data based on the standard deviation is plotted as well. Here the *1-σ* uncertainties are depicted, resulting in the range of 5.5% for a droplet size of 30 µm. Furthermore, histograms of the LIF/Mie ratio distribution at certain droplet sizes (± 1 µm) are given in Fig. 5. The histograms of certain experimental data showed a log-normal behavior (see section 3.1).

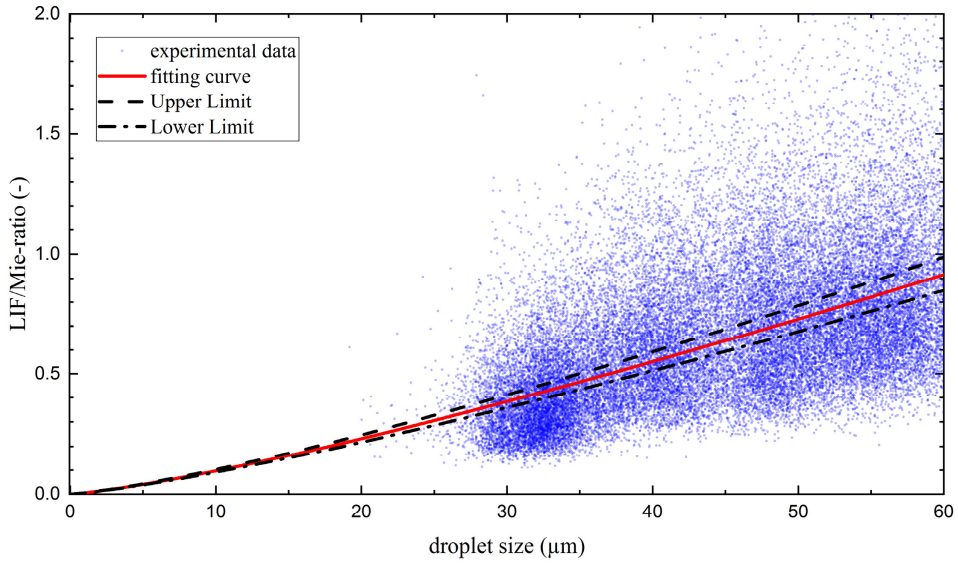

Fig. 4. The microscopic fitting curve (red) with the corresponding experimental data of single droplets plotted for LIF/Mie ratio as a function of droplet diameter for the reference conditions (0.1 MPa, 293 K, eosin concentration in ethanol: 0.5 vol %). The curves of the standard deviation are presented as well.

Optics EXPRESS

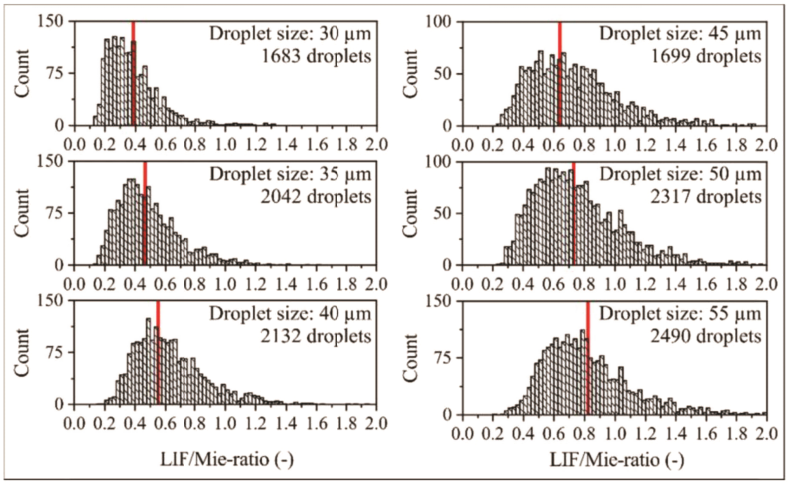

Fig. 5. The histograms of the LIF/Mie ratio distribution are provided and the corresponding fit value (red) for certain droplet sizes (± 1 µm).

3.3 Comparison between microscopic and macroscopic measurements

For the macroscopic measurements, the window of the CVC chamber was kept in between the droplet generator and the camera objective for comparable optical conditions of calibration and spray measurements. A distance of 225 mm between the objective and the light sheet was fixed and the same field-of-view was realized within the spray and the droplet generator. Figure 6 shows the simultaneous single-shot images of LIF and Mie signals recorded with micro/macro detections. The zoomed view of the images from the macroscopic setup shows the setup's ability to resolve the individual signals properly. The image post-processing described in subsection 3.1, applies only to the droplets which are within the chosen limits (sphericity etc.) and which can be detected with both micro and macro setups. With the microscopic setup, the LIF signal appears quite homogeneous through the droplet although few bright spots are visible. The macroscopic LIF-signal of the single droplet shows one large bright spot. From these single droplet data, the LIF/Mie ratio is calculated for all single droplets and the average curve is obtained from that.

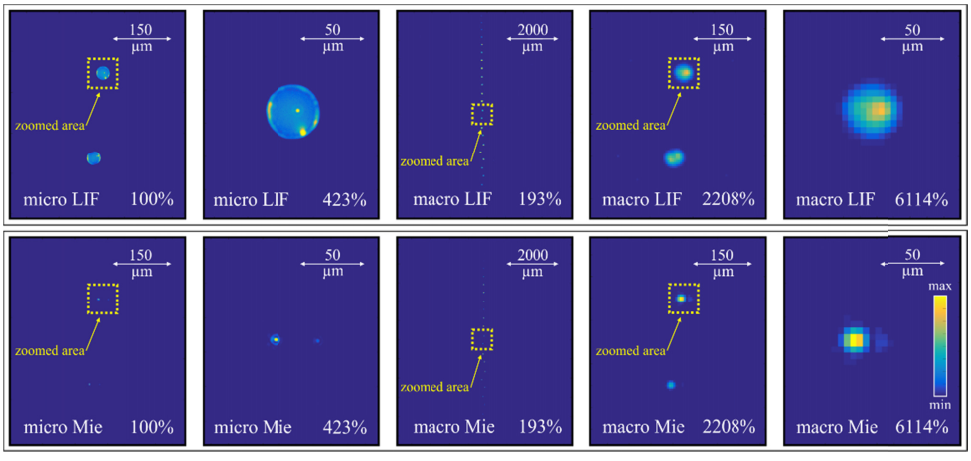

Fig. 6. Simultaneous micro/macroscopic LIF (top row) and Mie images (bottom row) of ethanol droplets (0.5 vol% eosin, 293 K). The percentage represents the zooming factor for better comparison of the droplet representation.

Optics EXPRESS

Figure 7 shows the resulting LIF/Mie ratio intensity curves as a function of droplet diameter for both micro and macro detections. The corresponding curve fitting parameters are given in Table 3. In both cases, the ratio curves show an approximately linear dependence on droplet diameter. There are some deviations between the two detections, which could be due to the lower spatial resolution in case of macroscopic imaging and opposite light collection angle. Nevertheless, the effects of the decreased resolution of the macroscopic detection, and the detection angle dependence of the Mie signal are found negligible for the ratio calibration in the existing setup. The macroscopic measurements are more realistic for the planar droplet sizing in sprays, therefore, results from the macroscopic investigations are only discussed further in this article. The macroscopic calibration curve for ethanol with 0.5 vol% eosin at 0.1 MPa, 293 K and 100% laser power is used as a reference in the following investigations.

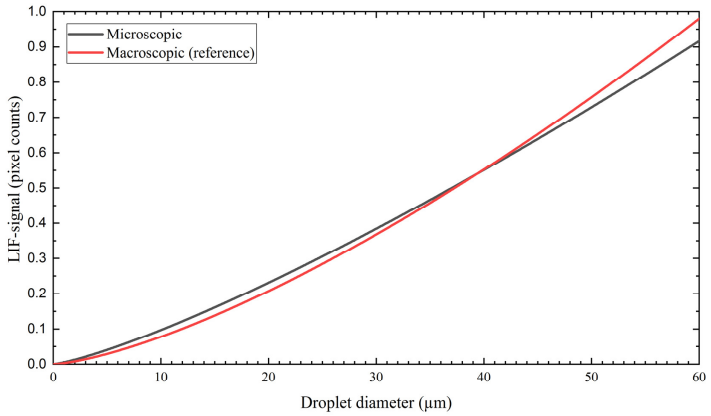

Fig. 7. The micro and macro (reference marked red) LIF/Mie ratio plotted as a function of droplet diameter. The deviations between the two detections is due to loss of resolution in macroscopic system and opposite collection angle.

Table 3. Microscopic and macroscopic LIF/Mie ratio curve fitting parameters for the pre-factor A and exponent b including the standard deviation for 0.5 vol% eosin 0.5 vol% at 293 K (reference marked grey).

signal fit	A	std. deviation A	b	std. deviation b
Micro LIF/Mie	0.0054	1.0371	1.2539	0.0096
Macro LIF/Mie	0.0030	1.0445	1.4139	0.0115

4. Effects of laser energy, dye concentration and liquid temperature

4.1 Effects of laser energy/fluence

The effects of laser energy variation are investigated at constant dye concentration (0.5 vol %) and temperature (293 K) for the macroscopic LIF/Mie ratio. Three output laser powers of 75%, 100% and 125% corresponding to laser fluences of 39.8 mJ/cm^2, 53.0 mJ/cm^2 and 66.3 mJ/cm^2 are investigated. The laser power variations are listed in Table 4.

Table 4. Variation of laser energy/fluence at constant dye concentration and temperature (reference marked grey).

Laser output power (%)	Laser pulse energy (mJ/pulse)	Laser fluence (mJ/cm^2)
75	3.04	39.8
100	4.05	53.0
125	5.06	66.3

Optics EXPRESS

Figure 8 shows the pulse energy variation as a function of the LIF/Mie ratio. At the lowest output energy (75%), the lower LIF and Mie intensity leads to lower signal to noise ratio. Therefore, the noise from the ratio also contributes to the ratio, yielding a higher exponent of the fitting curve (see Table 5). In general, there are small effects of laser energy on the ratio, which is similar to what has been reported for point measurements [36] and 2D measurements in sprays [32]. For a droplet diameter of 30 µm, the variation introduced by the laser fluence is about 8.3% as marked in Fig. 8 for a large laser energy variation of 25%.

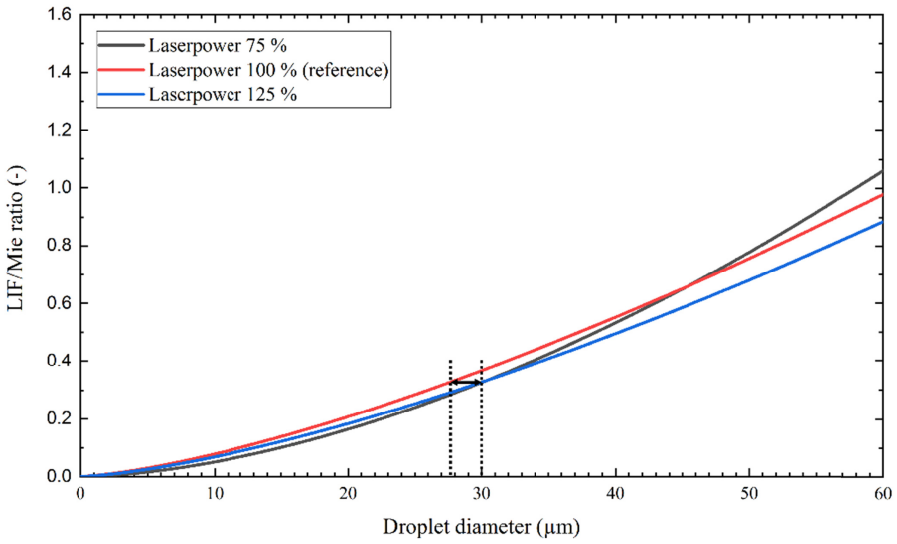

Fig. 8. Effects of laser power variation (reference marked red) on the macroscopic LIF/Mie ratio at constant dye concentration and fuel temperature. In general, there are small effects of laser power variation.

4.2 Effects of dye concentration

The effects of dye tracer eosin concentration are investigated at 0.25 vol %, 0.5 vol % and 0.75 vol % of the fuel at constant laser energy (100%) and fuel temperature (293 K). Figure 9 shows that an increase of the dye concentration leads to a proportional increase in the LIF/Mie ratio. For example, a three times increase in dye concentration results in an increase by a factor of 3.1 in the ratio for 30 µm diameter and by a factor of 4.9 for 60 µm droplets. This trend is expected from the LIF-signal dependency on the dye concentration as long as the fluorescence remains in the linear regime. Additionally, an increased dye concentration leads to a slightly larger extinction within the droplets, which again results in a slightly decreased Mie signal of the droplets. The dye concentration investigations by Mishra et al. also revealed that a three times increase in concentration increases “smaller” LIF/Mie ratio of 0.15 to 0.5 (3.33 times), while “larger” LIF/Mie ratio of 0.35 to 1.5 (4.28 times) [32].

At very high droplet temperatures, the dye concentration inside the droplet may vary with time due to evaporation of the fuel. In [34] a 3D-spray simulation was performed for a similar ethanol spray as it is investigated here (but for a different injection pressure). The simulation showed that 8% of ethanol evaporates within 2.4 milliseconds. This means that the average dye concentration in the droplet would increase from 0.5 to 0.54%. Assuming an increase of 10% in dye concentration (e.g. from 0.5 to 0.55) due to evaporation in the present case, this would result in an overestimated droplet size of about 6.7%.

Optics EXPRESS

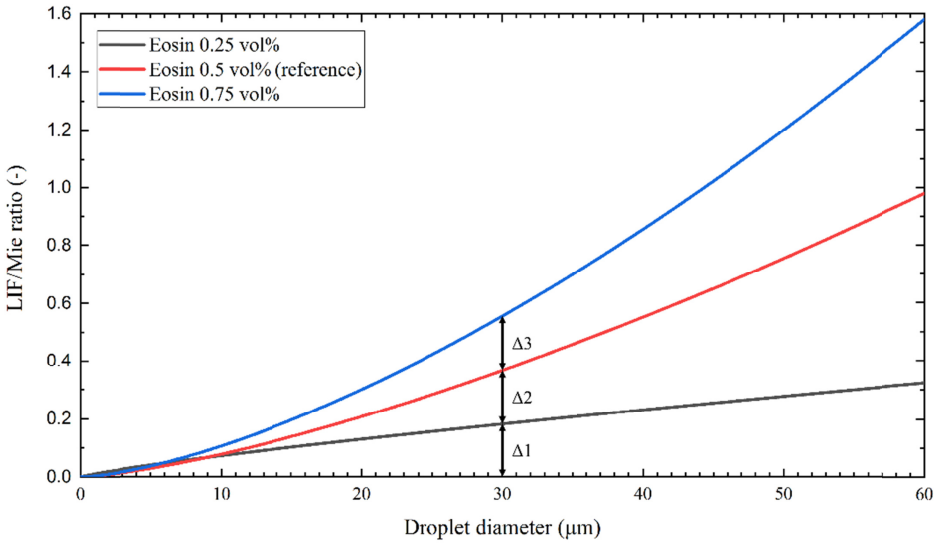

Fig. 9. Effects of dye concentration (reference marked red) for macroscopic LIF/Mie ratio as a function of droplet diameter. The three times increase in dye concentration leads 3.08 times increase in the ratio for 30 µm droplet.

4.3 Effects of liquid temperature

Figure 10 shows the effects of liquid temperature variation at constant laser energy (100%) and the dye concentration (0.5 vol. %). The LIF/Mie ratio is studied for three temperatures between 253 K and 333 K. The LIF/Mie ratio increases with an increase in fuel temperature. Earlier investigations in a cuvette showed, that a temperature change of 28 K between 296 and 324 K leads to a 7% difference in the LIF-signal [34]. Thus, a temperature increase of 40 K would result in a 10% higher LIF signal (when assuming a linear dependency). This corresponds roughly to the increase of the LIF/Mie ratio when the temperature is increased from 253 K to 293 K (which is about 15%, e.g. for a droplet size of 30 µm) in Fig. 10. This increased LIF-signal can be explained by the larger absorption cross section at increased temperatures which is typical for many fuel tracers [19]. Consequently, the larger absorption in the droplet would result in reduced Mie-scattering intensity and thus further increased LIF/Mie ratio. However, for further increased temperatures (at 333 K), there is a large increase of the LIF/Mie ratio compared to the lower temperatures 253 K and 293 K. The increase in LIF/Mie ratio is about 40% between 293 K and 333 K (for a 30 µm droplet). This can be explained as follows: The high temperature combined with the low boiling point of ethanol (see Table 1) results in partial evaporation of the ethanol droplets (which occurs between the nozzle and the studied ROI downstream the nozzle). Therefore, the dye concentration in the droplet increase while the droplet evaporates, leading to a high LIF, but low Mie signal, yielding a much higher LIF/Mie ratio. (However, it should be noted that in the ROI still the correct droplet size appears as it is controlled by using the microscopic sizing setup). Thus, large uncertainties up to 29% in droplet size may occur (for constant LIF/Mie ratio, as indicated by the arrows in Fig. 10) for large droplet temperature variations of 40 K and tracer enrichment due to evaporation.

Droplet temperature variations in a spray as studied below are expected to be much smaller (in the range of 10 K) as discussed in [34]. Assuming an average reduction of the droplet temperature of 10 K this would result in an overestimation of the droplet size by about 4%.

Optics EXPRESS

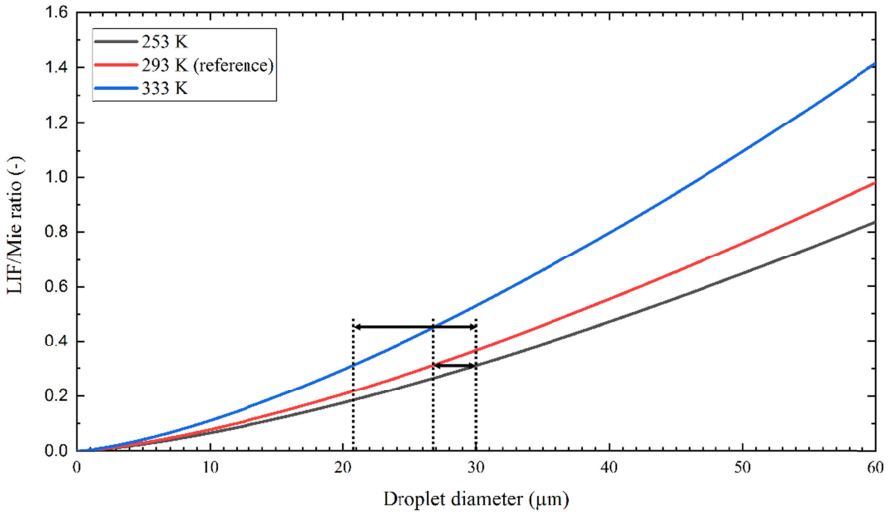

Fig. 10. Effects of liquid temperature variation on macroscopic LIF/Mie ratio (reference marked red) at constant laser power and dye concentration. The ratio increases at higher temperature of 333 K due to evaporation of the fuel. Under these elevated temperature conditions, the dye remains in the droplet while droplet diameter shrinks. Therefore, LIF signal increases but Mie signal decreases, yielding higher ratio. At the lower temperatures, evaporation is negligible but the small temperature effect in LIF is mainly responsible for the ratio increase.

The specific parameters for the fitting curves shown in subsections 4.1, 4.2 and 4.3 are listed in Table 5. In general, the standard errors of the exponents show a lower variation for the LIF signal fit in comparison to the Mie signal fit. This behavior is mainly due to isotropic radiation intensity in LIF compared to size dependent oscillations in Mie signals (see also the discussion in section 6).

Table 5. The curve fitting parameters for macroscopic LIF/Mie ratio as the effects of laser power, dye concentration and liquid temperature (reference marked grey).

Eosin (vol %)	Laser power (%)	Temperature	*a*	*b*
0.5	75	293 K	0.001	1.7019
0.5	100	293 K	0.003	1.4139
0.5	125	293 K	0.0025	1.4337
0.5	100	253 K	0.0025	1.4197
0.5	100	333 K	0.0042	1.4214
0.25	100	293 K	0.0107	0.8326
0.75	100	293 K	0.0033	1.5073

5. Results from the spray measurements

5.1 Single-shot 2D SMD maps of DISI sprays

For the calibration of the SLIPI-LIF/Mie ratio, the macroscopic plot is used (see Fig. 7). To resolve a single droplet in the droplet chain, the macroscopic objective (see camera position 2 in Fig. 1) is fixed at 225 mm. To cover the full DISI spray the objective (camera position 1 in Fig. 1) needs to be fixed at 915 mm from the incident light sheet. Therefore, the macroscopic LIF/Mie ratio is investigated for the objective at distances 225 mm to 915 mm. The observed variation in LIF/Mie for the two distances is not significant (less than 2.5%, not shown here),

Optics EXPRESS

therefore, the calibrated LIF/Mie ratio from single droplet at 225 mm can be used for the SLIPI-LIF/Mie ratio calibration.

Figure 11 shows calibrated single-shot SLIPI-LIF/Mie ratios converted as 2D maps of droplet SMD in DISI sprays at one point in time, which is at 2552 µs aVSOI (after visible start of injection). The dye concentration is 0.5 vol%, while the output laser power and liquid temperatures correspond to 100% and 293 K, respectively. The existence of ligaments in the near nozzle region (0 mm to 10 mm) is not considered for the SMD mapping. This means that droplets are not spherical in these regions and calculated SMD values are not realistic. The large droplets at the radial spray edges are in the range of 25-35 µm. The droplets at the spray front are in a range of 50 µm and larger, which is mainly caused by droplet coalescence mechanisms.

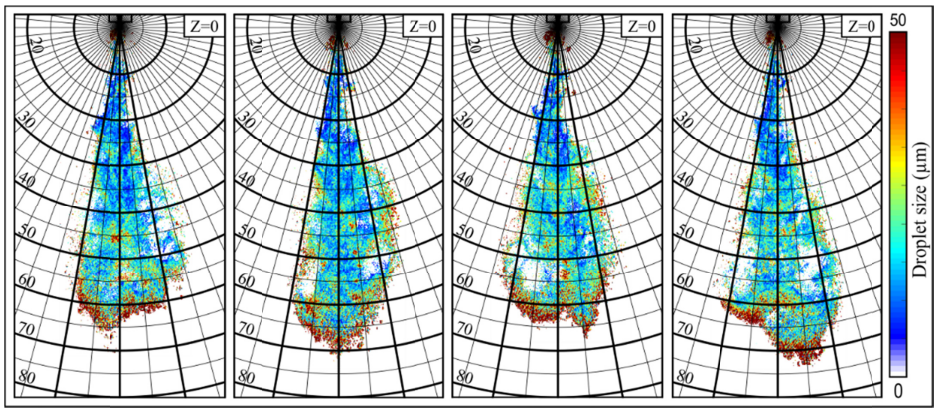

Fig. 11. Left: Calibrated SLIPI-LIF/Mie ratio single shot images representing the 2D droplet SMD distribution of a DISI ethanol fuel spray studied at 0.2 MPa chamber pressure, 16 MPa injection pressure, 293 K fuel and ambient temperature. Droplet SMD ranges from a minimum of 2 µm to a maximum of 50 µm.

6. Discussion of the Mie-scattering data

In this section, the presented Mie-scattering measurements as well as the chosen fitting curves are discussed. The Mie-scattering of individual droplets shows strong intensity fluctuations and it is very sensitive to the angle of detection and the droplet size. Thus it does actually not follow a potential trend [12,44,45] as mentioned in section 4. Furthermore, the ideal conditions of the Mie-theory (droplets are fixed within a specific point) are not covered in the experiments, because the locations of the individual droplets within the ROI are always different. This effect causes a variation of the detection angle of the droplets. However, angular smoothing, caused by the angular aperture of the detection system, leads to smaller intensity oscillations. Figure 12 shows the calculation of the Mie scattering signal for a droplet size from 1 to 60 µm for a detection angle of 90° with the microscopic angular aperture of 5.8° and the corresponding fitting curves for the calculations and the experiment. The specific parameters for the curve fitting are listed in Table 6.

Table 6. Normalized microscopic Mie curve fitting parameters for the experimental data and the calculations for the pre-factor A and exponent b including the standard deviation for 0.5 vol% eosin 0.5 vol% at 293 K

signal fit	A	std. deviation A	b	std. deviation b
Micro Mie experiment	0.0020	1.0471	2.1166	0.0123
Micro Mie calculation	0.0025	1.1605	1.8839	0.0391

Optics EXPRESS

The simulation was performed using a Matlab-algorithm based on the one presented by Bohren and Huffmann [46]. For the curve fitting the same routines as for the experimental data are used.

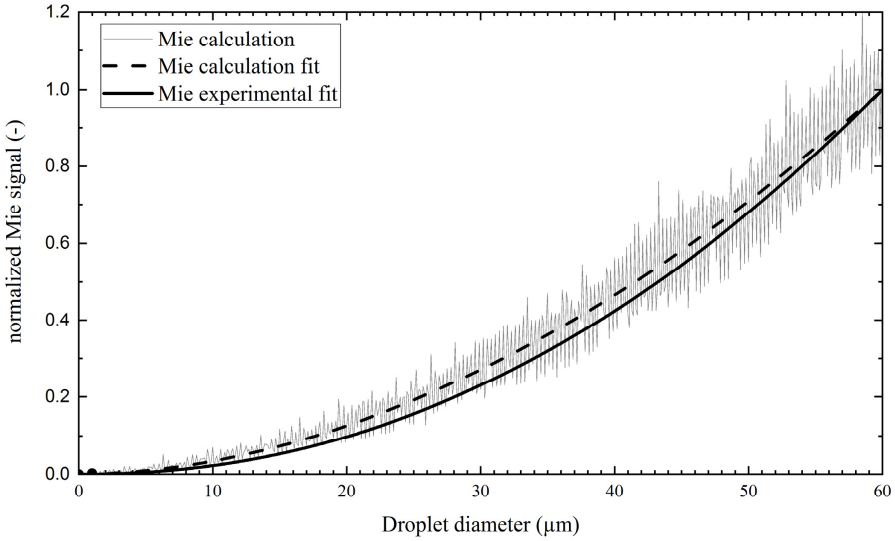

Fig. 12. The calculated Mie signal for the microscopic detection and the fitting curves of the calculated and the experimental Mie signal (0.1 MPa, 293 K, eosin concentration in ethanol: 0.5 vol %).

In principle, the Mie-scattering calculation still shows the above-mentioned strong intensity fluctuations. However, the highly angle dependent Mie-signal gets smoothened by the averaging over the detection angle of the camera. In general, the fitting curves of the calculated and the experimental data show a good agreement. For a 30 µm droplet, the deviation is in the range of 8%. Thus, this smoothing effect confirms the chosen post-processing algorithm according to section 3.1 based on a fitting to a potential function. Furthermore, Hofeldt *et al.* [44] also concluded that the integration over a continuous distribution in wavelength or diameter space will smoothen the scattered light intensities of the individual particles. Similar conclusions are also reported by Charalampous *et al.* [12]. Another experimental technique to reduce intensity oscillations within the Mie-scattering is the usage of femtosecond lasers as reported in [47] which also relies on the above mentioned effects.

7. Summary and conclusion

Monodisperse droplets of ethanol doped with eosin as a LIF tracer were studied with a long range microscope system. The droplets were produced using the flow-focusing mechanism, which results in droplets with high sphericity and a diameter ranging between 21 and 60 µm (although much larger droplets can be generated), which is relevant for engine spray conditions. The experimental data of the individual LIF, Mie signals and LIF/Mie ratio is fitted according to the power-law function $I = a \cdot d^b$. The Mie-scattering of individual droplets is highly sensitive to the angle of detection and the droplet size and does actually not follow a potential trend. A calculation of the Mie scattering intensity showed strong intensity oscillations of the Mie-signal with droplet size. However, the chosen detection angle smoothens the signal oscillations and allows the usage of a potential fitting procedure. Thus dye eosin with 0.5 vol % in ethanol showed a good agreement with the d^3- and d^2-dependence relation of the LIF- and Mie- signals, respectively. These microscopic measurements were simultaneously performed in combination with another macroscopic

Optics EXPRESS

objective, and for the comparison between the two detection schemes a total number of 33,510 droplets were evaluated for the reference experiment.

The macroscopic investigations of the droplet generator can be summarized as follows: (i) There is very minor influence of laser power variation (at constant dye concentration and liquid temperature) on the LIF/Mie ratio. (ii) The variation of the dye concentration (at constant laser power and liquid temperature) showed a strong dependence of the LIF signal and a weak effect on Mie-signal on the amount of dye within the droplets leading to strong dependence on LIF/Mie ratio. Thus, for reliable droplet sizing with the current investigation, a constant dye concentration is required (i.e. evaporation and dye enrichment in the droplet should be reduced). (iii) The LIF/Mie ratio increases with an increase in fuel temperature. The larger variation in the ratio is observed at 333 K in comparison to temperatures at 253 K and 293 K. The investigated maximum temperature of 333 K is extremely high for the utilized fuel. This leads to an increase of the dye concentration within the droplets due to evaporation of ethanol. This is because the dye used is a solid and remains in the droplet. Accordingly, the technique is not applicable for high temperature environments and high evaporation rates. If the requirement and conditions such as constant dye concentration, and almost iso-thermal fuel temperatures are respected, the macroscopic LIF/Mie ratio of the droplet generator can be directly used to calibrate SLIPI-LIF/Mie ratio in other technical and IC engine sprays. In this case, the *1-σ* uncertainty of the calibration data was determined to be 5.5% for droplet sizes of 30 µm.

The results from the spray measurement are as follows: (i) Instantaneous 2D mapping of droplet SMD field is extracted with the investigated method. (ii) Droplet SMD for the probed DISI spray varies between 5 to 50 µm at 293 K liquid temperature. The droplet SMD at the radial positions in spray edges are in the range of 5 µm to 40 µm. The droplets at the spray front are in the range 25-50 and higher, which is mainly due coalescence mechanisms. It is important to mention that the use of different fuels might affect the LIF/Mie ratio. For example, previous study of using butanol and ethanol as base fuels showed strong deviations of the LIF/Mie ratio calibration curves based on PDA calibration [34]. Therefore, effects of the fuel on LIF/Mie ratio will be part of future studies using droplet generator experiments that will be addressed in a subsequent publication.

Finally, the LIF/Mie ratio calibration setup in combination with SLIPI-based droplet sizing can measure droplet SMD in much faster and more reliable manner than in comparison to conventional PDS and PDA measurements. The setup can be used for layer-wise 2D and averaged 3D mapping of SMD in engine sprays and the other technical sprays employed for industrial applications.

Funding

German Federal Ministry of Food and Agriculture (BMEL) through the Agency for Renewable Resources (FNR), FKZ: 22026711; German Research Foundation (DFG); European Research Council (ERC) under the European Union's Horizon 2020 research and innovation program (Agreement No. 638546—ERC starting grant "Spray-Imaging").

Acknowledgement

Erlangen Graduate School in Advanced Optical Technologies (SAOT).

References

1. C.-N. Yeh, H. Kosaka, and T. Kamimoto, "Fluorescence/scattering image technique for particle sizing in unsteady diesel spray," Transactions of the Japan Society of Mechanical Engineers Series B **59**(568), 4008–4013 (1993).
2. P. Le Gal, N. Farrugia, and D. A. Greenhalgh, "Laser Sheet Dropsizing of dense sprays," Opt. Laser Technol. **31**(1), 75–83 (1999).
3. A. Malarski, B. Schürer, I. Schmitz, L. Zigan, A. Flügel, and A. Leipertz, "Laser sheet dropsizing based on two-dimensional Raman and Mie scattering," Appl. Opt. **48**(10), 1853–1860 (2009).

Optics EXPRESS

4. W. Zeng, M. Xu, Y. Zhang, and Z. Wang, "Laser sheet dropsizing of evaporating sprays using simultaneous LIEF/MIE techniques," Proc. Combust. Inst. **34**(1), 1677–1685 (2013).
5. A. Serpengüzel, S. Küçükşenel, and R. Chang, "Microdroplet identification and size measurement in sprays with lasing images," Opt. Express **10**(20), 1118–1132 (2002).
6. R. Domann and Y. Hardalupas, "Quantitative Measurement of Planar Droplet Sauter Mean Diameter in Sprays using Planar Droplet Sizing," Particle & Particle Systems Characterization **20**(3), 209–218 (2003).
7. R. Domann and Y. Hardalupas, "Spatial distribution of fluorescence intensity within large droplets and its dependence on dye concentration," Appl. Opt. **40**(21), 3586–3597 (2001).
8. R. Domann, Y. Hardalupas, and A. R. Jones, "A study of the influence of absorption on the spatial distribution of fluorescence intensity within large droplets using Mie theory, geometrical optics and imaging experiments," Meas. Sci. Technol. **13**(3), 280–291 (2002).
9. B. Frackowiak and C. Tropea, "Fluorescence modeling of droplets intersecting a focused laser beam," Opt. Lett. **35**(9), 1386–1388 (2010).
10. B. Frackowiak and C. Tropea, "Numerical analysis of diameter influence on droplet fluorescence," Appl. Opt. **49**(12), 2363–2370 (2010).
11. G. Charalampous and Y. Hardalupas, "Method to reduce errors of droplet sizing based on the ratio of fluorescent and scattered light intensities (laser-induced fluorescence/Mie technique)," Appl. Opt. **50**(20), 3622–3637 (2011).
12. G. Charalampous and Y. Hardalupas, "Numerical evaluation of droplet sizing based on the ratio of fluorescent and scattered light intensities (LIF/Mie technique)," Appl. Opt. **50**(9), 1197–1209 (2011).
13. G. Charalampous, Y. Hardalupas, and A. M. K. P. Taylor, "Novel Technique for Measurements of Continuous Liquid Jet Core in an Atomizer," AIAA J. **47**, 2605–2615 (2009).
14. R. Domann and Y. Hardalupas, "A Study of Parameters that Influence the Accuracy of the Planar Droplet Sizing (PDS) Technique," Particle & Particle Systems Characterization **18**(1), 3–11 (2001).
15. W. Chaze, O. Caballina, G. Castanet, and F. Lemoine, "The saturation of the fluorescence and its consequences for laser-induced fluorescence thermometry in liquid flows," Exp. Fluids **57**(4), 58 (2016).
16. K. Matsumoto, T. Fujii, K. Suzuki, D. Segawa, and T. Kadota, "Laser-induced fluorescence for the non-intrusive diagnostics of a fuel droplet burning under microgravity in a drop shaft," Meas. Sci. Technol. **10**(10), 853–858 (1999).
17. M. Winter and L. A. Melton, "Measurement of internal circulation in droplets using laser-induced fluorescence," Appl. Opt. **29**(31), 4574–4577 (1990).
18. P. Lavieille, F. Lemoine, G. Lavergne, and M. Lebouché, "Evaporating and combusting droplet temperature measurements using two-color laser-induced fluorescence," Exp. Fluids **31**(1), 45–55 (2001).
19. I. Düwel, J. Schorr, J. Wolfrum, and C. Schulz, "Laser-induced fluorescence of tracers dissolved in evaporating droplets," Appl. Phys. B **78**, 127–131 (2004).
20. K. Jung, H. Koh, and Y. Yoon, "Assessment of planar liquid-laser-induced fluorescence measurements for spray mass distributions of like-doublet injectors," Meas. Sci. Technol. **14**(8), 1387–1395 (2003).
21. J. Trost, L. Zigan, and A. Leipertz, "Quantitative vapor temperature imaging in DISI-sprays at elevated pressures and temperatures using two-line excitation laser-induced fluorescence," Proc. Combust. Inst. **34**(2), 3645–3652 (2013).
22. B. D. Stojkovic and V. Sick, "Evolution and impingement of an automotive fuel spray investigated with simultaneous Mie/LIF techniques," Appl. Phys. B **73**(1), 75–83 (2001).
23. M. Storch, S. Lind, S. Will, and L. Zigan, "Influence of ethanol admixture on the determination of equivalence ratios in DISI engines by laser-induced fluorescence," Appl. Opt. **55**(30), 8532–8540 (2016).
24. M. Storch, Y. N. Mishra, M. Koegl, E. Kristensson, S. Will, L. Zigan, and E. Berrocal, "Two-phase SLIPI for instantaneous LIF and Mie imaging of transient fuel sprays," Opt. Lett. **41**(23), 5422–5425 (2016).
25. E. Berrocal, E. Kristensson, and L. Zigan, "Light sheet fluorescence microscopic imaging for high-resolution visualization of spray dynamics," Int. J. Spray Combust. Dyn. **10**(1), 86–98 (2018).
26. Y. N. Mishra, E. Kristensson, M. Koegl, J. Jönsson, L. Zigan, and E. Berrocal, "Comparison between two-phase and one-phase SLIPI for instantaneous imaging of transient sprays," Exp. Fluids **58**(9), 110 (2017).
27. X.-F. Zhang, J. Zhang, and L. Liu, "Fluorescence Properties of Twenty Fluorescein Derivatives: Lifetime, Quantum Yield, Absorption and Emission Spectra," J. Fluoresc. **24**(3), 819–826 (2014).
28. S. V. Sankar, K. E. Maher, D. M. Robart, and W. D. Bachalo, "Rapid Characterization of Fuel Atomizers Using an Optical Patternator," J. Eng. Gas Turbine. Power **121**(3), 409–414 (1999).
29. M. C. Jermy and D. A. Greenhalgh, "Planar dropsizing by elastic and fluorescence scattering in sprays too dense for phase Doppler measurement," Appl. Phys. B **71**(5), 703–710 (2000).
30. J. Zelina, A. Rodrigue, and S. Sankar, "Fuel injector characterization using laser diagnostics at atmospheric and elevated pressures," in *36th AIAA Aerospace Sciences Meeting and Exhibit* (American Institute of Aeronautics and Astronautics, 1998).
31. M. Zaller, R. J. Locke, and R. C. Anderson, "Comparison of techniques for non-intrusive fuel drop size measurements in a subscale gas turbine combustor," J. Vis. (Tokyo) **2**(3-4), 301–308 (2000).
32. Y. N. Mishra, E. Kristensson, and E. Berrocal, "Reliable LIF/Mie droplet sizing in sprays using structured laser illumination planar imaging," Opt. Express **22**(4), 4480–4492 (2014).

Optics EXPRESS

33. Y. N. Mishra, E. Kristensson, and E. Berrocal, "3D droplet sizing and 2D optical depth measurements in sprays using SLIPI based techniques," in *the 18th International Symposium on the Application of Laser and Imaging Techniques to Fluid Mechanics-LISBON Symposium*, Lisbon 2016)
34. M. Koegl, Y. N. Mishra, M. Storch, C. Conrad, E. Berrocal, S. Will, and L. Zigan, "Analysis of ethanol and butanol direct-injection spark-ignition sprays using two-phase structured laser illumination planar imaging droplet sizing," Int. J. Spray Combust. Dyn. **2018**, 1756827718772496 (2018).
35. H. Duan, F. Romay, Z. Syedain, B. Y. H. Liu, and A. Naqwi, "A New Monodisperse Droplet Generator and its Applications," ILASS Americas 28th Annual Conference on Liquid Atomization and Spray Systems (2016).
36. S. Park, H. Cho, I. Yoon, and K. Min, "Measurement of droplet size distribution of gasoline direct injection spray by droplet generator and planar image technique," Meas. Sci. Technol. **13**(6), 859–864 (2002).
37. J. A. Dean, *Lange's Handbook of Chemistry,* 15th ed. (McGraw-Hill Companies, 1999).
38. A. Richard, Yetter and I. Glassman, *Combustion,* 4th ed. (Academic Press, Amsterdam, 2008).
39. N. I. o. S. a. Technology, "NIST Chemistry WebBook," (2017).
40. J. Rheims, J. Köser, and T. Wriedt, "Refractive-index measurements in the near-IR using an Abbe refractometer," Meas. Sci. Technol. **8**(6), 601–605 (1997).
41. H. El-Kashef, "The necessary requirements imposed on polar dielectric laser dye solvents," Physica B **279**(4), 295–301 (2000).
42. J. Palmer, M. A. Reddemann, V. Kirsch, and R. Kneer, "Applying 2D-2cLIF-EET thermometry for micro-droplet internal temperature imaging," Exp. Fluids **59**(3), 51 (2018).
43. M. Anand, A. K. Dharmadhikari, J. A. Dharmadhikari, A. Mishra, D. Mathur, and M. Krishnamurthy, "Two-photon pumped lasing from methanol micro-droplets doped by a weakly fluorescent dye," Chem. Phys. Lett. **372**(1-2), 263–268 (2003).
44. D. L. Hofeldt, "Full-field measurements of particle size distributions: I. theoretical limitations of the polarization ratio method," Appl. Opt. **32**(36), 7551–7558 (1993).
45. C. Tropea, "Optical particle characterization in flows," Annu. Rev. Fluid Mech. **43**(1), 399–426 (2011).
46. C. F. Bohren and D. R. Huffmann, *Absorption and Scattering of Light by Small Particles* (Wiley, New York, 1983).
47. S. Bareiss, B. Bork, S. Bakić, C. Tropea, R. Irsig, J. Tiggesbäumker, and A. Dreizler, "Application of femtosecond lasers to the polarization ratio technique for droplet sizing," Meas. Sci. Technol. **24**(2), 025203 (2013).